

Data-Driven Decomposition of Conservative and Non-Conservative Dynamics in Multiscale Systems

Ludovico Theo Giorgini*

Department of Mathematics, Massachusetts Institute of Technology,
Cambridge, MA 02139, USA

May 6, 2025

Abstract

We present a data-driven framework for reconstructing physics-consistent reduced models of multiscale systems. Our approach addresses a fundamental challenge in model reduction: decomposing the deterministic drift into its conservative (reversible) and non-conservative (irreversible) components while preserving the system’s invariant measure and autocorrelation. We leverage the k-means Gaussian-mixture method (KGMM) to robustly estimate the score function—the gradient of the logarithm of the steady-state probability density. This score function is then combined with a finite-volume discretization of the Perron–Frobenius generator to identify a drift matrix whose symmetric part captures the conservative dynamics and whose antisymmetric part encodes the minimal irreversible circulation required by the empirical data. The result is a reduced Langevin model that preserves the stationary density, reproduces short-time correlations by construction, and maintains computational efficiency. We validate our framework on three increasingly complex systems: a one-dimensional nonlinear stochastic system with multiplicative noise, a two-dimensional asymmetric four-well potential system with non-gradient drift, and the stochastic Lorenz-63 attractor. In all cases, our surrogate models accurately recover both the stationary distribution and autocorrelation structure of the original dynamics, while providing an interpretable separation of conservative and non-conservative forces.

1 Introduction

Many natural and engineered systems evolve on a hierarchy of temporal and spatial scales that render direct numerical simulation prohibitively expensive. In such settings, *reduced-order stochastic models* serve a dual purpose: they distill the essential macroscopic behaviour of the full dynamics and furnish an interpretable mathematical description amenable to rigorous analysis. Stochastic reduced-order models are particularly valuable tools across numerous disciplines, especially in climate science, contributing significantly to both the comprehension and forecasting of system dynamics [1, 2, 3, 4, 5, 6, 7, 8, 9, 10, 11, 12, 13].

*Email: ludogio@mit.edu

Classical closure strategies—ranging from homogenisation and Mori–Zwanzig projection [14, 15] to energy-conserving parametric ansätze [16]—achieve this goal under restrictive assumptions, most notably scale separation or weak nonlinear coupling [17]. Contemporary data-driven approaches circumvent these limitations by learning the governing laws directly from time series, yet frequently sacrifice physical consistency: the reconstructed drift may generate spurious long-time statistics that destroy invariant measures [18, 19]. Modern clustering-based algorithms have shown that statistical properties of multiscale dynamical systems can be estimated more reliably from coarse-grained observational data than the systems’ detailed dynamical trajectories [20, 21, 22, 23, 24, 25, 26].

Our approach leverages coarse-grained observational data to construct a physically consistent reduced order model based on two fundamental components: the score function—the gradient of the logarithm of the steady-state probability density—that encodes the steady-state probability distribution and a drift matrix that captures temporal correlations while preserving conservation laws. For the score function estimation, we employ the *k-means Gaussian-mixture method* (KGMM) introduced in our previous work [27], which combines statistical density estimation with machine learning by approximating the steady state through a Gaussian mixture model and partitioning the state space with k-means clustering. From the same coarse-grained data, we construct the drift matrix using a finite-volume discretization of the Perron–Frobenius generator, identifying both conservative and non-conservative components of the dynamics. This data-driven approach ensures by construction that the resulting Langevin model preserves both the empirical stationary density and autocorrelation structure of the observed data.

We validate the framework on three prototypical multiscale systems of increasing complexity: a one-dimensional nonlinear stochastic differential equation (SDE) exhibiting multiplicative noise, a two-dimensional asymmetric double-well potential system with non-gradient drift, and the stochastic Lorenz–63 attractor. In each case the surrogate accurately recovers both the stationary probability distribution and the autocorrelation structure of the original dynamics, while offering an analytically transparent partition of reversible and irreversible forces.

The paper is organized as follows: in Section 2 we present the method, including the decomposition of the Langevin dynamics into conservative and non-conservative components, the construction of the score function using KGMM, and the construction of the drift matrix. In Section 3 we present the results of applying our method to three different stochastic dynamical systems. Finally, in Section 4 we conclude with a summary of our findings and potential future directions.

2 Method

2.1 Conservative and Non-Conservative Components in the Langevin Dynamics

We consider the stochastic differential equation:

$$\dot{\vec{x}}(t) = \vec{F}(\vec{x}) + \sqrt{2}\Sigma \vec{\xi}(t), \quad (1)$$

where $\vec{x}(t) \in \mathbb{R}^D$ is the state vector, $\vec{F} : \mathbb{R}^D \rightarrow \mathbb{R}^D$ is the deterministic drift, $\Sigma \in \mathbb{R}^{D \times D}$ is a positive definite diffusion matrix, and $\vec{\xi}(t)$ represents Gaussian white noise with zero mean and unit variance.

The evolution of the probability density $p(\vec{x}, t)$ associated with this stochastic process is described by the Fokker–Planck equation:

$$\frac{\partial p}{\partial t} = -\vec{\nabla} \cdot [\vec{F}(\vec{x}) p] + \vec{\nabla} \cdot [\Sigma \Sigma^T \vec{\nabla} p]. \quad (2)$$

Assuming the existence of a smooth steady-state distribution $p_S(\vec{x})$, the stationary condition $\partial_t p_S = 0$ leads to:

$$0 = -\vec{\nabla} \cdot [\vec{F}(\vec{x}) p_S(\vec{x})] + \vec{\nabla} \cdot [\Sigma \Sigma^T \vec{\nabla} p_S(\vec{x})]. \quad (3)$$

Rearranging terms, we obtain:

$$\vec{\nabla} \cdot \left[\left(\vec{F}(\vec{x}) - \Sigma \Sigma^T \vec{\nabla} \ln p_S(\vec{x}) \right) p_S(\vec{x}) \right] = 0. \quad (4)$$

This suggests that the drift $\vec{F}(\vec{x})$ can be decomposed into two components:

$$\vec{F}(\vec{x}) = \Sigma \Sigma^T \vec{\nabla} \ln p_S(\vec{x}) + \vec{g}(\vec{x}), \quad (5)$$

where the first term represents the conservative (time-reversible) component, and the second term, $\vec{g}(\vec{x})$, represents the non-conservative (time-irreversible) component.

The non-conservative term $\vec{g}(\vec{x})$ satisfies the following constraint:

$$\vec{\nabla} \cdot (\vec{g}(\vec{x}) p_S(\vec{x})) = 0, \quad (6)$$

or equivalently:

$$\vec{\nabla} \cdot \vec{g}(\vec{x}) + \vec{g}(\vec{x}) \cdot \vec{\nabla} \ln p_S(\vec{x}) = 0. \quad (7)$$

We now analyze the structure of $\vec{g}(\vec{x})$ and use a representation that satisfies the constraint in Eq. (7). Specifically, we express $\vec{g}(\vec{x})$ in terms of an antisymmetric tensor field $\mathbf{R}(\vec{x})$ and the effective potential $V(\vec{x}) = -\ln p_S(\vec{x})$:

$$\vec{g}(\vec{x}) = \vec{\nabla} \cdot \mathbf{R}(\vec{x}) - \mathbf{R}(\vec{x}) \vec{\nabla} V(\vec{x}), \quad (8)$$

where $\mathbf{R}(\vec{x})$ satisfies the antisymmetry condition:

$$\mathbf{R}(\vec{x})^T = -\mathbf{R}(\vec{x}). \quad (9)$$

For a detailed demonstration that this representation satisfies Eq. (7), see Appendix A. Furthermore, if \vec{g} is divergence-free, we have:

$$\begin{aligned} \vec{g} &= \vec{\nabla} \cdot \mathbf{R} - \mathbf{R} \vec{\nabla} V, \\ 0 &= (\vec{\nabla} \cdot \mathbf{R}) \cdot \vec{\nabla} V. \end{aligned} \quad (10)$$

Since now \vec{g} is perpendicular to $\vec{\nabla} V$, we can write it as:

$$\vec{g} = \mathbf{R}_{df} \vec{\nabla} V, \quad (11)$$

where the redefined antisymmetric tensor field \mathbf{R}_{df} is given by the *wedge-formula*:

$$\mathbf{R}_{df}(\vec{x}) = \frac{1}{S(\vec{x})} \left(\vec{g}(\vec{x}) \vec{\nabla} V(\vec{x})^T - \vec{\nabla} V(\vec{x}) \vec{g}(\vec{x})^T \right), \quad (12)$$

where $S(\vec{x}) = \|\vec{\nabla}V\|^2$.

We decompose $\mathbf{R}(\vec{x})$ into a mean and a fluctuation part:

$$\mathbf{R}(\vec{x}) = -\tilde{\mathbf{R}} + \delta\mathbf{R}(\vec{x}), \quad (13)$$

where $\tilde{\mathbf{R}} = -\langle\mathbf{R}\rangle$ is minus the temporal average of $\mathbf{R}(\vec{x})$ over the domain, and $\delta\mathbf{R}(\vec{x})$ represents the residual fluctuations. Assuming that $\delta\mathbf{R}(\vec{x})$ is small, we approximate:

$$\vec{g}(\vec{x}) \approx \tilde{\mathbf{R}}\vec{\nabla}V(\vec{x}). \quad (14)$$

One checks directly that this approximation satisfies the continuity constraint in Eq. (6):

Substituting this approximation into the Langevin equation, we obtain the reduced dynamics:

$$\dot{\vec{x}}(t) = \left(\Sigma\Sigma^T + \tilde{\mathbf{R}}\right)\vec{\nabla}\ln p_S(\vec{x}) + \sqrt{2}\Sigma\vec{\xi}(t). \quad (15)$$

In this reduced model, the irreversible effects of the original dynamics are incorporated as an effective antisymmetric correction to the conservative drift term.

We now rewrite the drift term $\Sigma\Sigma^T + \tilde{\mathbf{R}}$ as Φ , where the drift matrix Φ is decomposed into symmetric and antisymmetric parts:

$$\Phi = \Phi_S + \Phi_A, \quad (16)$$

where $\Phi_S = \Sigma\Sigma^T = \frac{1}{2}(\Phi + \Phi^T)$ is the symmetric part and $\Phi_A = \tilde{\mathbf{R}} = \frac{1}{2}(\Phi - \Phi^T)$ is the antisymmetric part.

The Langevin equation can now be rewritten as:

$$\dot{\vec{x}}(t) = \Phi\vec{\nabla}\ln p_S(\vec{x}) + \sqrt{2}\Sigma\vec{\xi}(t), \quad (17)$$

where Σ is related to Φ_S by the Cholesky decomposition:

$$\Sigma = \text{cholesky}(\Phi_S). \quad (18)$$

This formulation separates the reversible (symmetric) and irreversible (antisymmetric) contributions to the dynamics, with Φ_S governing the equilibrium-like behavior and Φ_A encoding the circulation or flux patterns characteristic of nonequilibrium steady states.

2.2 Score Function Estimation via KGMM

In this subsection, we summarize the KGMM algorithm presented in [27] for robust estimation of the score function $\vec{s}(\vec{x}) = \vec{\nabla}\ln p_S(\vec{x})$, which is directly related to the effective potential $V(\vec{x}) = -\ln p_S(\vec{x})$ described in the previous section. The score function plays a fundamental role in statistical physics, dynamical systems, and machine learning, underpinning the Generalized Fluctuation-Dissipation Theorem (GFDT) that connects spontaneous fluctuations to system responses [28, 29, 30, 31, 32, 33], generative modeling [34], parameter estimation [35], and causal inference tasks [36]. In our framework, we employ the score function to construct the deterministic drift term in the reduced Langevin dynamics, ensuring that the resulting model preserves the system's invariant measure.

The KGMM method approximates the probability density $p(\vec{x})$ as a Gaussian Mixture Model (GMM) [27]:

$$p(\vec{x}) = \frac{1}{N} \sum_{i=1}^N \mathcal{N}(\vec{x} \mid \vec{\mu}_i, \sigma_G^2 \mathbf{I}), \quad (19)$$

where $\vec{\mu}_i$ are data points sampled from the steady-state distribution $p_S(\vec{x})$, and σ_G^2 is the isotropic covariance of the Gaussian kernels. The corresponding score function is given by:

$$\vec{\nabla} \ln p(\vec{x}) = -\frac{1}{\sigma_G^2} \sum_{i=1}^N \frac{\mathcal{N}(\vec{x} \mid \vec{\mu}_i, \sigma_G^2 \mathbf{I})(\vec{x} - \vec{\mu}_i)}{p(\vec{x})}. \quad (20)$$

However, this direct computation becomes numerically unstable for small σ_G , as the density and its gradient become highly sensitive to local fluctuations in the data.

To address this issue, KGMM leverages a probabilistic identity. If $\vec{x} = \vec{\mu} + \sigma_G \vec{z}$, where $\vec{z} \sim \mathcal{N}(\vec{0}, \mathbf{I})$, the score function can be expressed as:

$$\vec{\nabla} \ln p(\vec{x}) = -\frac{1}{\sigma_G^2} \mathbb{E}[\vec{z} \mid \vec{x}]. \quad (21)$$

This identity allows the score function to be computed as the conditional expectation of the kernel displacements \vec{z} , scaled by $-1/\sigma_G^2$.

The KGMM algorithm estimates the score function empirically through the following steps:

1. Perturb the original data points $\{\vec{\mu}_i\}$ by adding Gaussian noise to generate perturbed samples $\vec{x}_i = \vec{\mu}_i + \sigma_G \vec{z}_i$, where $\vec{z}_i \sim \mathcal{N}(\vec{0}, \mathbf{I})$.
2. Partition the perturbed samples $\{\vec{x}_i\}$ into N_C control volumes $\{\Omega_j\}$ using bisecting K-means clustering. Let \vec{C}_j denote the centroid of cluster Ω_j .
3. For each cluster Ω_j , compute the conditional expectation of the displacements:

$$\mathbb{E}[\vec{z} \mid \vec{x} \in \Omega_j] \approx \frac{1}{|\Omega_j|} \sum_{i: \vec{x}_i \in \Omega_j} \vec{z}_i. \quad (22)$$

4. Estimate the score function at the cluster centroid \vec{C}_j as:

$$\vec{s}_j = \vec{\nabla} \ln p_S(\vec{C}_j) \approx -\frac{1}{\sigma_G^2} \mathbb{E}[\vec{z} \mid \vec{x} \in \Omega_j]. \quad (23)$$

5. Fit a neural network to interpolate the discrete score estimates $\{(\vec{C}_j, \vec{s}_j)\}$ across the entire domain.

The number of clusters N_C must be chosen carefully to balance resolution and noise. A practical scaling relation is:

$$N_C \propto \sigma_G^{-D}, \quad (24)$$

where D is the effective dimensionality of the data, and σ_G is the kernel width. This ensures that clusters remain small enough to capture local gradient structure while containing enough points for robust averaging.

The choice of σ_G is critical. Smaller values of σ_G yield score estimates closer to the true steady-state distribution but increase statistical noise. Larger values smooth out fluctuations, improving stability but introducing bias. The optimal σ_G balances these competing effects, minimizing bias while maintaining statistical reliability.

2.3 Construction of the Drift Matrix

To construct the drift matrix Φ , which governs the effective dynamics, we approximate the generator of the Perron–Frobenius operator with the rate matrix, using a finite-volume discretization. The state space is partitioned into the same N_C control volumes used in the previous subsection to construct the score function, with \vec{C}_i , $i \in [1, N_C]$ denoting the center of each control volume.

To define the rate matrix $\mathbf{Q} \in \mathbb{R}^{N_C \times N_C}$, we consider the evolution of the probability vector $\vec{\rho}(t)$, where each component $\rho_i(t)$ represents the probability of the system being in control volume Ω_i at time t . The dynamics of $\vec{\rho}(t)$ is governed by the equation:

$$\dot{\vec{\rho}} = \mathbf{Q} \vec{\rho}. \quad (25)$$

The off-diagonal elements Q_{ij} represent the transition rates from volume j to volume i , while the diagonal elements are determined by the conservation of probability:

$$Q_{ii} = - \sum_{j \neq i} Q_{ji}. \quad (26)$$

Empirical transition counts among the control volumes, obtained from short-time trajectory data, define the rate matrix. The off-diagonal entries of \mathbf{Q} capture the rates of transitions from volume j to volume i , while the diagonal entries are determined to enforce row sums of zero, ensuring probability conservation. The resulting discrete steady-state probability density function $\vec{\pi}$ satisfies:

$$\mathbf{Q} \vec{\pi} = \vec{0}, \quad (27)$$

which is the stationary condition for the Markov process. For more details on the construction of the rate matrix, see [23, 24].

Let x_i^n denote the i -th component of the center of bin n , with stationary probability mass π_n . From the discrete rate matrix \mathbf{Q} , the short-time correlation functions for small τ can be written as [23, 24]:

$$\lim_{\tau \rightarrow 0} C_{ij}(\tau) = \sum_{n=1}^{N_C} x_j^n \pi_n \sum_{m=1}^{N_C} x_i^m [e^{\mathbf{Q} \tau}]_{mn} \quad (28)$$

$$\approx \sum_{n=1}^{N_C} x_j^n \pi_n \sum_{m=1}^{N_C} x_i^m [\mathbf{I} + \mathbf{Q} \tau]_{mn}. \quad (29)$$

Simultaneously, the Langevin system (17) with drift $\Phi \vec{\nabla} \ln p_S$ predicts the following short-time expansion:

$$\lim_{\tau \rightarrow 0} C_{ij}(\tau) \approx \sum_{n=1}^{N_C} x_j^n \pi_n \left(x_i^n + [\Phi \vec{s}_n]_i \tau \right). \quad (30)$$

Matching terms order-by-order in τ , we obtain:

$$\sum_{n,m=1}^{N_C} x_j^n \pi_n x_i^m Q_{mn} = \sum_{n=1}^{N_C} x_j^n \pi_n [\Phi \vec{s}_n]_i. \quad (31)$$

Define the following matrices:

$$M_{i,j} := \sum_{n,m=1}^{N_C} x_j^n \pi_n x_i^m Q_{mn}, \quad V_{j,k} := \sum_{n=1}^{N_C} x_j^n \pi_n [\vec{s}]_k. \quad (32)$$

Then, the relationship between these matrices is:

$$M_{i,j} = \sum_{k=1}^{N_C} [\Phi]_{i,k} V_{j,k}, \quad \Rightarrow \quad \mathbf{M} = \Phi \mathbf{V}^T. \quad (33)$$

If \mathbf{V} is invertible (or can be pseudoinverted), we can solve for Φ :

$$\Phi = \mathbf{M} (\mathbf{V}^T)^{-1}. \quad (34)$$

This equation provides a systematic way to construct the drift matrix Φ from the empirical transition rates and the estimated score function. The resulting drift matrix captures both the conservative and non-conservative components of the dynamics, allowing for a physically consistent representation of the system.

3 Results

We tested the proposed algorithm presented in Section 2 for constructing both the score function and Φ on three different stochastic dynamical systems relevant in climate science. Similar systems were previously studied in [27]. Here, we demonstrate how our approach provides a stochastic model capable of reproducing both the autocorrelation functions (ACFs) and probability density functions (PDFs) directly from data. For each system, we used the estimated score function and Φ to generate stochastic trajectories by integrating the following Langevin equation:

$$\dot{\vec{x}}(t) = \Phi \vec{\nabla} \ln \rho_S(\vec{x}) + \sqrt{2} \Sigma \vec{\xi}(t), \quad (35)$$

where $\Phi = \Phi_S + \Phi_A$ is the decomposition of the drift matrix into symmetric and anti-symmetric parts, Σ is related to Φ_S by the Cholesky decomposition, and $\vec{\xi}(t)$ is a vector of independent delta-correlated Gaussian white noise processes.

Each system was simulated over a time interval $T \in [0, 10^5 t_d]$, where t_d denotes the decorrelation time of the system. These datasets were subsequently used to train the KGMM-based score function estimation method. For each system, we employed a three-layer neural network with 128 and 64 neurons in the first and second hidden layers, respectively. We used the Swish activation function between the first two layers, and a linear activation function for the output layer.

The three systems studied are as follows:

- **One-Dimensional Nonlinear SDE:** This is a one-dimensional system, and therefore, the drift term only has a conservative component (antisymmetric tensors cannot exist in one dimension). The system is described by:

$$\dot{x}(t) = F + ax(t) + bx^2(t) - cx^3(t) + \sigma_1 \xi_1(t) + \sigma_2(x) \xi_2(t), \quad (36)$$

where the coefficients are:

$$\begin{aligned} a &= -1.809, & b &= -0.0667, & c &= 0.1667, \\ A &= 0.1265, & B &= -0.6325, & F &= \frac{AB}{2}, \\ \sigma_1 &= 0.0632, & \sigma_2(x) &= A - Bx. \end{aligned} \quad (37)$$

We used $N_C = 76$, $\sigma_G = 0.05$ inside the KGMM algorithm described in Section 2.

The method successfully reproduced both the PDF and ACF of the system, as shown in Fig. 1. The reconstructed dynamics used a Langevin equation with additive noise to approximate one with multiplicative noise.

- **Two-Dimensional Asymmetric Potential System:** This system has both conservative and non-conservative components in the drift. The system is described by:

$$\dot{\vec{x}}(t) = -\mathbf{K}\vec{\nabla}U(\vec{x}) + \sqrt{2}\vec{\xi}(t), \quad (38)$$

where the potential function $U(\vec{x})$ is:

$$U(\vec{x}) = (x_1 + A_1)^2(x_1 - A_1)^2 + (x_2 + A_2)^2(x_2 - A_2)^2 + B_1x_1 + B_2x_2, \quad (39)$$

and the matrix \mathbf{K} introduces a rotational component:

$$\mathbf{K} = \begin{pmatrix} 1 & -0.8 \\ 0.8 & 1 \end{pmatrix}. \quad (40)$$

The parameters are:

$$A_1 = 1.0, \quad A_2 = 1.2, \quad B_1 = 0.6, \quad B_2 = 0.3. \quad (41)$$

We used $N_C = 761$, $\sigma_G = 0.05$ inside the KGMM algorithm described in Section 2. Since the fluctuations of \mathbf{R} around its mean are zero by construction, the approximation of \mathbf{R} with a constant antisymmetric tensor in Section 2 is exact. The figure demonstrates that our method accurately reproduced both the PDFs and ACFs, as shown in Fig. 2.

- **Stochastic Lorenz-63 Model:** The system is described by:

$$\begin{aligned} \dot{x}_1(t) &= \sigma(x_2(t) - x_1(t)) + \sigma_\xi\xi_1(t), \\ \dot{x}_2(t) &= x_1(t)(\rho - x_3(t)) - x_2(t) + \sigma_\xi\xi_2(t), \\ \dot{x}_3(t) &= x_1(t)x_2(t) - \beta x_3(t) + \sigma_\xi\xi_3(t), \end{aligned} \quad (42)$$

where the coefficients are:

$$\sigma = 10.0, \quad \rho = 28.0, \quad \beta = \frac{8}{3}, \quad \sigma_\xi = 5.0. \quad (43)$$

We used $N_C = 762$, $\sigma_G = 0.05$ inside the KGMM algorithm described in Section 2. In this case, the fluctuations of \mathbf{R} around its mean are non-zero (see Appendix B), and the approximation of \mathbf{R} with a constant antisymmetric tensor is not exact. The figure shows that while the approximation is not precise, the results are still useful. All the PDFs are recovered precisely. The ACFs for the first two dimensions match well, while for the third dimension, the ACF does not recover the oscillations but follows the maxima of the peaks, as shown in Fig. 3.

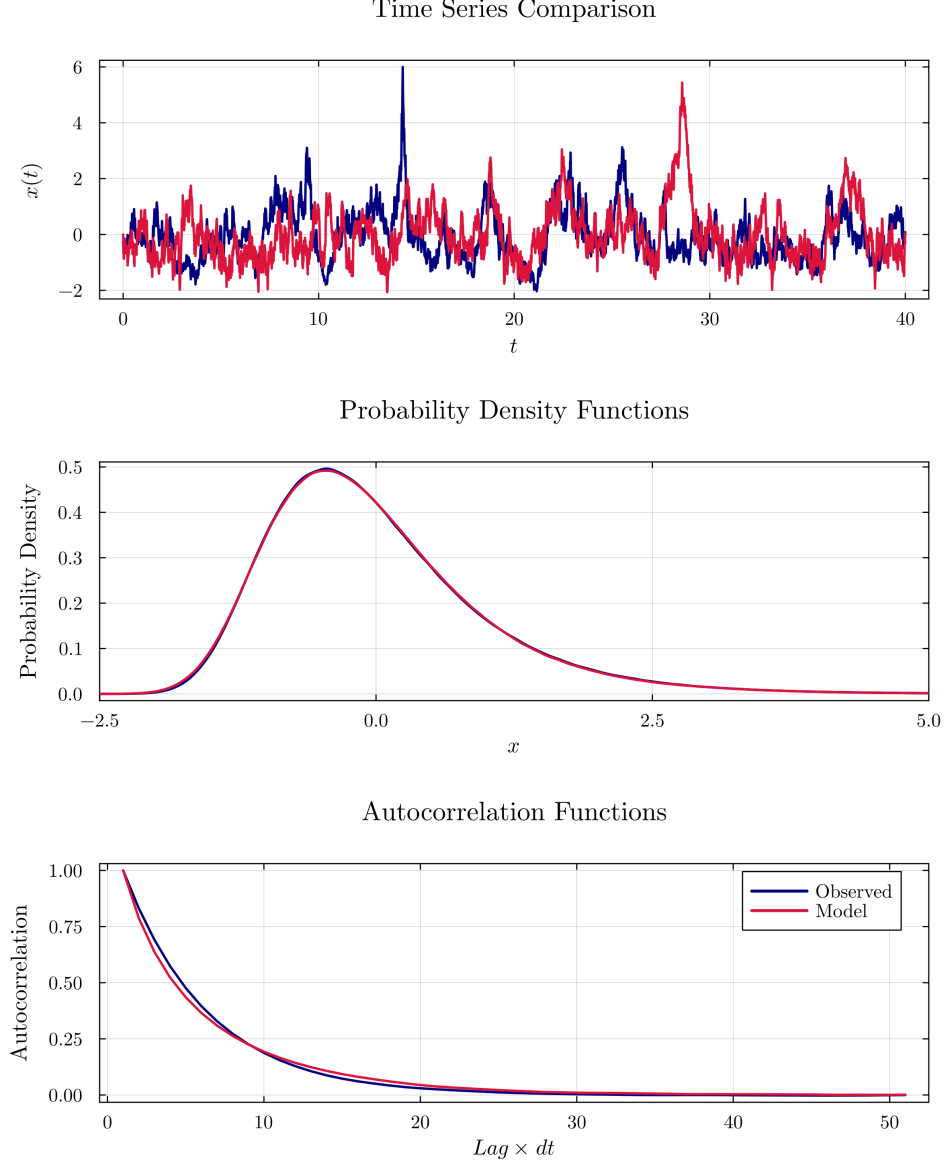


Figure 1: **First row:** Time series comparison between the original system (Observed) and the reconstructed dynamics (Model) using the KGMM score function and Φ . The same noise realization has been used to generate both time series. **Second row:** Comparison of the observed marginal PDFs (blue) with the reconstructed PDFs (red) obtained from the Langevin equation using the KGMM score function and Φ . **Third row:** Comparison of the observed ACFs (blue) with the reconstructed ACFs (red).

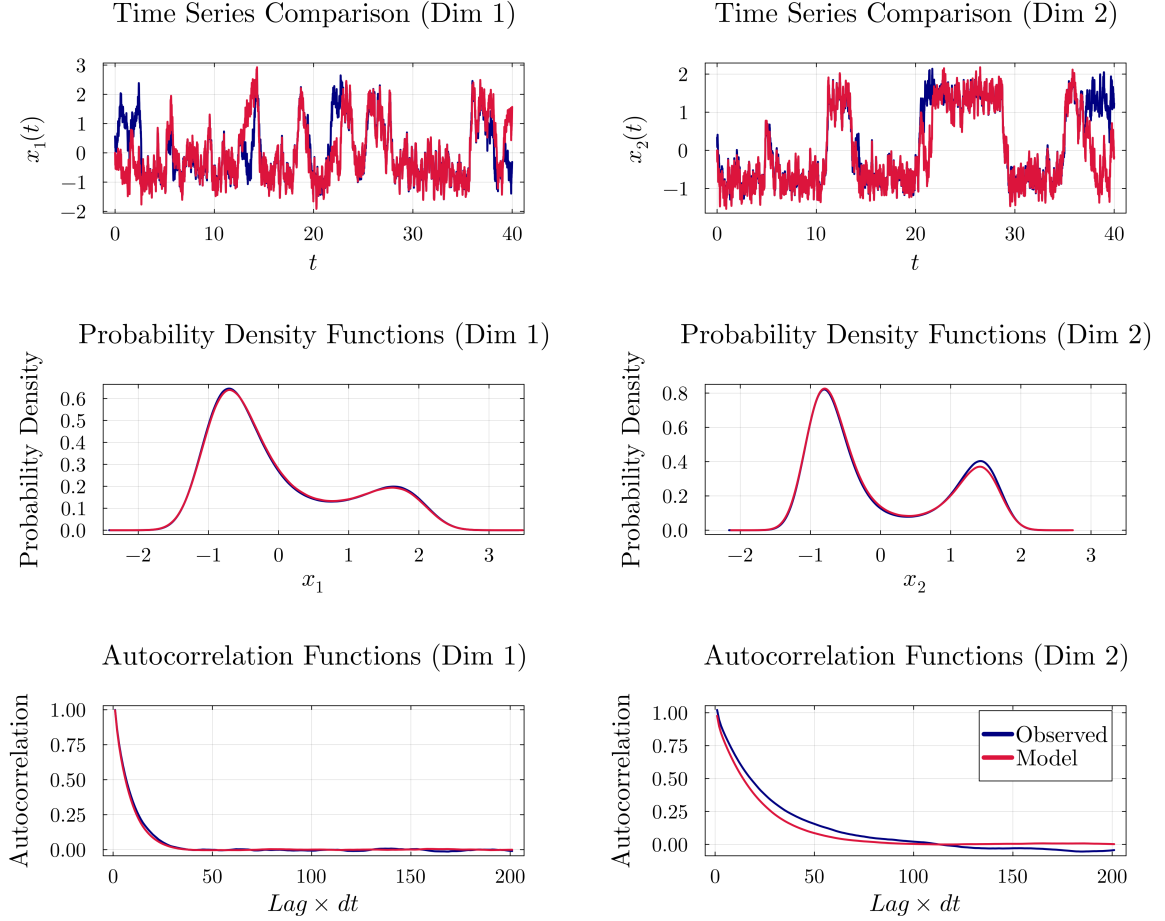


Figure 2: **Two-dimensional asymmetric potential system. First row:** Comparison of trajectories between the original system (Observed) and the reconstructed dynamics (Model) using the KGMM score function and Φ . The same noise realization has been used to generate both time series. **Second row:** Comparison of the observed marginal PDFs (blue) with the reconstructed PDFs (red) for each variable. **Third row:** Comparison of the observed ACFs (blue) with the reconstructed ACFs (red) for each variable.

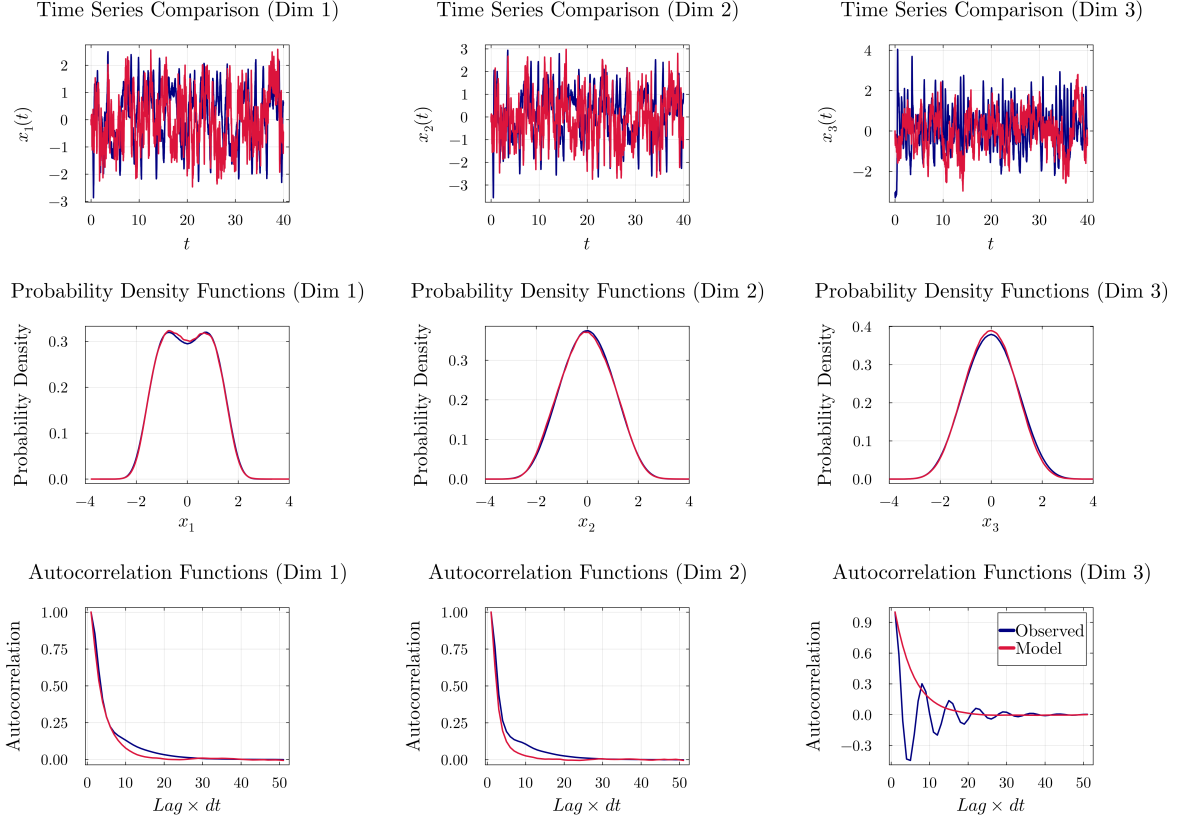


Figure 3: **Lorenz 63 system. First row:** Time series comparison between the original chaotic system (Observed) and the reconstructed dynamics (Model) using the KGMM score function and Φ . The same noise realization has been used to generate both time series. **Second row:** Comparison of the observed marginal PDFs (blue) with the reconstructed marginal PDFs (red) for x_1 , x_2 , and x_3 . **Third row:** Comparison of the observed ACFs (blue) with the reconstructed ACFs (red) for each variable.

4 Conclusions

In this paper, we have presented a data-driven framework for reconstructing physically consistent reduced-order models of multiscale stochastic systems through explicit separation of conservative and non-conservative components of the dynamics. Our approach successfully addresses two fundamental challenges in model reduction: robustly estimating the score function from empirical data and enforcing the continuity constraint required for the non-conservative component of the drift. These challenges are critical for building models that faithfully reproduce both the system’s invariant measure and autocorrelation functions across various timescales.

The KGMM algorithm effectively handles the score function estimation by leveraging conditional expectation identities and dimension-adaptive clustering, providing numerical stability even at small kernel bandwidths where traditional methods fail. This estimated score function, combined with our finite-volume reconstruction of the Perron-Frobenius generator, enables the identification of a drift matrix Φ whose symmetric and antisymmetric parts respectively encode the system’s conservative and irreversible dynamics. A key aspect of our approach is the approximation of the non-conservative part of the drift with its spatial average, which significantly simplifies the reconstruction while maintaining the essential features of the dynamics. This decomposition ensures that the reduced model generates trajectories consistent with both the empirical steady-state distribution and short-time correlations of the original system.

Our validation across three progressively complex dynamical systems reveals both strengths and limitations of the approach. For the one-dimensional nonlinear SDE and two-dimensional asymmetric potential system, the method achieved exceptional accuracy in reproducing both probability densities and autocorrelation functions. In the more challenging stochastic Lorenz-63 system, where the antisymmetric tensor field varies significantly across state space, our constant- \mathbf{R} approximation successfully captured the marginal distributions and reproduces the autocorrelation structure of the first two variables with high fidelity, though with some limitations in fully capturing oscillatory patterns in the third dimension.

The framework offers several advantages over existing techniques. Unlike direct drift estimation methods, our approach guarantees preservation of the invariant measure. Compared to parametric techniques, it doesn’t require prior knowledge of the functional form of the dynamics. The explicit decomposition into conservative and non-conservative components provides physical interpretability, allowing researchers to distinguish between processes driving the system toward equilibrium and those maintaining non-equilibrium circulation patterns.

Future work could extend in several promising directions. First, improving the framework to handle non-constant antisymmetric tensor fields would enhance performance on complex systems like Lorenz-63. Second, incorporating memory effects would enable capturing non-Markovian behaviors that arise in model reduction scenarios with partially observed data. Third, applying this methodology to real-world observational data from climate and geophysical fluid dynamics could yield valuable reduced-order descriptions of Earth system processes, potentially improving climate projections and our understanding of critical transitions.

Acknowledgments

We thank Andre Souza for useful discussions.

Appendix

A Verification of the Decomposition of $\vec{g}(\vec{x})$

To verify that this representation satisfies Eq. (7), we expand the divergence of $\vec{g}(\vec{x})$:

$$\begin{aligned}\vec{\nabla} \cdot \vec{g} &= \vec{\nabla} \cdot (\vec{\nabla} \cdot \mathbf{R}) - \vec{\nabla} \cdot (\mathbf{R} \vec{\nabla} V) \\ &= \underbrace{\vec{\nabla} \cdot (\vec{\nabla} \cdot \mathbf{R})}_A - \left[(\vec{\nabla} \cdot \mathbf{R}) \cdot \vec{\nabla} V + \langle \mathbf{R}, \vec{\nabla} \vec{\nabla} V \rangle \right].\end{aligned}\quad (44)$$

Here, we apply the product rule for divergence:

$$\vec{\nabla} \cdot (\mathbf{R} \vec{\nabla} V) = (\vec{\nabla} \cdot \mathbf{R}) \cdot \vec{\nabla} V + \sum_{i,j} R_{ij} \partial_i \partial_j V. \quad (45)$$

The second term can be written as the contraction of the antisymmetric tensor \mathbf{R} with the Hessian matrix of V , denoted as $\vec{\nabla} \vec{\nabla} V$. Since $R_{ij} = -R_{ji}$ is antisymmetric and $\partial_i \partial_j V = \partial_j \partial_i V$ is symmetric (assuming sufficient smoothness of V), this contraction vanishes:

$$\langle \mathbf{R}, \vec{\nabla} \vec{\nabla} V \rangle = \sum_{i,j} R_{ij} \partial_i \partial_j V = 0. \quad (46)$$

Additionally, for an antisymmetric tensor field \mathbf{R} with sufficiently smooth components, the double divergence vanishes identically:

$$\vec{\nabla} \cdot (\vec{\nabla} \cdot \mathbf{R}) = 0. \quad (47)$$

This can be verified directly using index notation and the antisymmetry property of \mathbf{R} . Substituting Eqs. (45) and (47) into the divergence of \vec{g} , we find:

$$\vec{\nabla} \cdot \vec{g} = -(\vec{\nabla} \cdot \mathbf{R}) \cdot \vec{\nabla} V. \quad (48)$$

Next, we compute the dot product $\vec{g} \cdot \vec{\nabla} V$:

$$\begin{aligned}\vec{g} \cdot \vec{\nabla} V &= \left[\vec{\nabla} \cdot \mathbf{R} - \mathbf{R} \vec{\nabla} V \right] \cdot \vec{\nabla} V \\ &= (\vec{\nabla} \cdot \mathbf{R}) \cdot \vec{\nabla} V - (\mathbf{R} \vec{\nabla} V) \cdot \vec{\nabla} V.\end{aligned}\quad (49)$$

Since \mathbf{R} is antisymmetric, the second term vanishes:

$$(\mathbf{R} \vec{\nabla} V) \cdot \vec{\nabla} V = \sum_{i,j} R_{ij} \partial_j V \partial_i V = - \sum_{i,j} R_{ji} \partial_i V \partial_j V = 0, \quad (50)$$

where we have used the antisymmetry relation $R_{ij} = -R_{ji}$ and the commutativity of the product $\partial_i V \partial_j V$. Thus, we obtain:

$$\vec{g} \cdot \vec{\nabla} V = (\vec{\nabla} \cdot \mathbf{R}) \cdot \vec{\nabla} V. \quad (51)$$

Combining the results for $\vec{\nabla} \cdot \vec{g}$ and $\vec{g} \cdot \vec{\nabla} V$, we find:

$$\begin{aligned} \vec{\nabla} \cdot \vec{g} + \vec{g} \cdot \vec{\nabla} V &= -(\vec{\nabla} \cdot \mathbf{R}) \cdot \vec{\nabla} V + (\vec{\nabla} \cdot \mathbf{R}) \cdot \vec{\nabla} V \\ &= 0. \end{aligned} \quad (52)$$

This confirms that the proposed decomposition of $\vec{g}(\vec{x})$ satisfies the required constraint in Eq. (7).

B Separation of Conservative and Non-Conservative Forcing for the Lorenz-63 System

We start from the deterministic Lorenz-63 vector field:

$$\vec{F}(x_1, x_2, x_3) = \begin{pmatrix} \sigma(x_2 - x_1) \\ x_1(\rho - x_3) - x_2 \\ x_1 x_2 - \beta x_3 \end{pmatrix}. \quad (53)$$

Define the quadratic potential

$$V(x_1, x_2, x_3) = \frac{1}{2} (\sigma x_1^2 + x_2^2 + \beta x_3^2), \quad (54)$$

so that the conservative (gradient) part is

$$-\vec{\nabla} V = \begin{pmatrix} -\sigma x_1 \\ -x_2 \\ -\beta x_3 \end{pmatrix}. \quad (55)$$

The non-conservative residual is then

$$\vec{g}(x_1, x_2, x_3) = \vec{F} + \vec{\nabla} V = \begin{pmatrix} \sigma x_2 \\ x_1(\rho - x_3) \\ x_1 x_2 \end{pmatrix}. \quad (56)$$

We seek an antisymmetric tensor field $\mathbf{R}(x_1, x_2, x_3)$, $\mathbf{R}^T = -\mathbf{R}$, satisfying

$$\vec{g}(x_1, x_2, x_3) = \underbrace{\vec{\nabla} \cdot \mathbf{R}(x_1, x_2, x_3)}_{(\partial_j R_{ji})} - \underbrace{\mathbf{R}(x_1, x_2, x_3) \vec{\nabla} V(x_1, x_2, x_3)}_{(R_{ij} \partial_j V)}. \quad (57)$$

In index notation this reads, for each $i = 1, 2, 3$,

$$g_i = \partial_j R_{ji} - R_{ij} \partial_j V, \quad (58)$$

with the antisymmetry conditions

$$R_{12} = -R_{21}, \quad R_{13} = -R_{31}, \quad R_{23} = -R_{32}. \quad (59)$$

Explicitly, the three scalar fields (R_{12}, R_{13}, R_{23}) must satisfy the coupled system:

$$\begin{cases} \partial_{x_2} R_{21} + \partial_{x_3} R_{31} - (R_{12} x_2 + R_{13} \beta x_3) = \sigma x_2, \\ \partial_{x_1} R_{12} + \partial_{x_3} R_{32} - (-R_{12} \sigma x_1 + R_{23} \beta x_3) = x_1 (\rho - x_3), \\ \partial_{x_1} R_{13} + \partial_{x_2} R_{23} - (-R_{13} \sigma x_1 - R_{23} x_2) = x_1 x_2. \end{cases} \quad (60)$$

In order to satisfy this coupled system, the entries of the matrix \mathbf{R} must be functions of the state variables.

References

- [1] K. Hasselmann. Stochastic climate models part i. theory. *Tellus*, 28:473–485, 1976.
- [2] C. Penland. Random Forcing and Forecasting Using Principal Oscillation Pattern Analysis. *Monthly Weather Review*, 117:2165–2185, 1989.
- [3] C. Penland and P.D. Sardeshmukh. The optimal growth of tropical sea surface temperature anomalies. *Journal of Climate*, 8(8):1999–2024, 1995.
- [4] A. J. Majda, I. Timofeyev, and Vanden-Eijnden. Models for stochastic climate prediction. *Proc. Natl. Acad. Sci. USA*, 96:14687–14691, 1999.
- [5] A. J. Majda, I. Timofeyev, and Vanden-Eijnden. A mathematical framework for stochastic climate models. *Proc. Natl. Acad. Sci. USA*, 54:891–974, 2001.
- [6] D. Kondrashov, M.D. Chekroun, and M. Ghil. Data-driven non-markovian closure models. *Physica D: Nonlinear Phenomena*, 297:33–55, 2015.
- [7] K. Strounine, S. Kravtsov, D. Kondrashov, and M. Ghil. Reduced models of atmospheric low-frequency variability: Parameter estimation and comparative performance. *Physica D: Nonlinear Phenomena*, 239(3):145–166, 2010.
- [8] V. Lucarini and M.D. Chekroun. Theoretical tools for understanding the climate crisis from Hasselmann’s programme and beyond. *Nat Rev Phys (2023)*, 2023.
- [9] S. Kravtsov, D. Kondrashov, and M. Ghil. Multilevel Regression Modeling of Non-linear Processes: Derivation and Applications to Climatic Variability . *Journal of Climate*, 18:4404–4424, 2005.
- [10] Andrew J Majda, Christian Franzke, and Boualem Khouider. An applied mathematics perspective on stochastic modelling for climate. *Philosophical Transactions of the Royal Society A: Mathematical, Physical and Engineering Sciences*, 366(1875):2427–2453, 2008.
- [11] Nan Chen, Xiao Hou, Qin Li, and Yingda Li. Understanding and predicting nonlinear turbulent dynamical systems with information theory. *Atmosphere*, 10(5):248, 2019.
- [12] N D Keyes, L T Giorgini, and J S Wettlaufer. Stochastic paleoclimatology: Modeling the epica ice core climate records. *Chaos*, 33(9):093132, 2023.
- [13] Ludovico T Giorgini, W Moon, N Chen, and J Wettlaufer. Non-gaussian stochastic dynamical model for the el niño southern oscillation. *Physical Review Research*, 4(2):L022065, 2022.
- [14] Grigorios A Pavliotis and Andrew Stuart. *Multiscale methods: averaging and homogenization*, volume 53. Springer Science & Business Media, 2008.
- [15] Alexandre J Chorin and Fei Lu. Discrete approach to stochastic parametrization and dimension reduction in nonlinear dynamics. *Proceedings of the National Academy of Sciences*, 112(32):9804–9809, 2015.

- [16] Sulian Thual, Andrew J Majda, Nan Chen, and Samuel N Stechmann. Simple stochastic model for el niño with westerly wind bursts. *Proceedings of the National Academy of Sciences*, 113(37):10245–10250, 2016.
- [17] Marc GD Geers, Varvara G Kouznetsova, and WAM1402 Brekelmans. Multi-scale computational homogenization: Trends and challenges. *Journal of computational and applied mathematics*, 234(7):2175–2182, 2010.
- [18] Jason A Platt, Stephen G Penny, Timothy A Smith, Tse-Chun Chen, and Henry DI Abarbanel. Constraining chaos: Enforcing dynamical invariants in the training of reservoir computers. *Chaos: An Interdisciplinary Journal of Nonlinear Science*, 33(10), 2023.
- [19] Jared L Callahan, Georgios Rigas, Jean-Christophe Loiseau, and Steven L Brunton. An empirical mean-field model of symmetry-breaking in a turbulent wake. *Science Advances*, 8(19):eabm4786, 2022.
- [20] Fabrizio Falasca, Pavel Perezhogin, and Laure Zanna. Data-driven dimensionality reduction and causal inference for spatiotemporal climate fields. *Physical Review E*, 109(4):044202, 2024.
- [21] F. Falasca, A. Basinski, L. Zanna, and M. Zhao. A fluctuation-dissipation theorem perspective on radiative responses to temperature perturbations. *Arxiv (Accepted, in Press in Journal of Climate)*, 2025.
- [22] Ludovico T Giorgini, Andre N Souza, Domenico Lippolis, Predrag Cvitanović, and Peter Schmid. Learning dissipation and instability fields from chaotic dynamics. *arXiv preprint arXiv:2502.03456*, 2025.
- [23] Ludovico T Giorgini, Andre N Souza, and Peter J Schmid. Reduced markovian models of dynamical systems. *Physica D: Non-linear Phenomena*, 470:134393, 2024.
- [24] Andre N Souza. Representing turbulent statistics with partitions of state space. part 1. theory and methodology. *Journal of Fluid Mechanics*, 997:A1, 2024.
- [25] Andre N Souza. Representing turbulent statistics with partitions of state space. part 2. the compressible euler equations. *Journal of Fluid Mechanics*, 997:A2, 2024.
- [26] Andre N. Souza and Simone Silvestri. A modified bisecting k-means for approximating transfer operators: Application to the lorenz equations. *arXiv preprint arXiv:2412.03734*, 2024. Submitted to arXiv on Dec 4, 2024.
- [27] Ludovico T Giorgini, Tobias Bischoff, and Andre N Souza. Kgmm: A k-means clustering approach to gaussian mixture modeling for score function estimation. *arXiv preprint arXiv:2503.18054*, 2025.
- [28] U. M. B. Marconi, A. Puglisi, L. Rondoni, and A. Vulpiani. Fluctuation-dissipation: Response theory in statistical physics. *Physics Reports*, 461(4-6):111–195, 2008.
- [29] Ludovico Theo Giorgini, Katherine Deck, Tobias Bischoff, and Andre Souza. Response theory via generative score modeling. *Physical Review Letters*, 133(26):267302, 2024.

- [30] Fenwick C Cooper and Peter H Haynes. Climate sensitivity via a nonparametric fluctuation–dissipation theorem. *Journal of the Atmospheric Sciences*, 68(5):937–953, 2011.
- [31] Marco Baldovin, Fabio Cecconi, and Angelo Vulpiani. Understanding causation via correlations and linear response theory. *Physical Review Research*, 2(4):043436, 2020.
- [32] Michael Ghil and Valerio Lucarini. The physics of climate variability and climate change. *Reviews of Modern Physics*, 92(3):035002, 2020.
- [33] Ludovico T Giorgini, Fabrizio Falasca, and Andre N Souza. Predicting forced responses of probability distributions via the fluctuation-dissipation theorem and generative modeling. *arXiv preprint arXiv:2504.13333*, 2025.
- [34] Yang Song, Jascha Sohl-Dickstein, Diederik P Kingma, Abhishek Kumar, Stefano Ermon, and Ben Poole. Score-based generative modeling through stochastic differential equations. *arXiv preprint arXiv:2011.13456*, 2021.
- [35] B. W. Silverman. *Density Estimation for Statistics and Data Analysis*. Chapman and Hall/CRC, 1986.
- [36] S. Shimizu, P.O. Hoyer, A. Hyvärinen, and A.J. Kerminen. A linear non-gaussian acyclic model for causal discovery. *Journal of Machine Learning Research*, 7:2003–2030, 2007.